

Experimental and Theoretical Measurements of the Evolution of Embryos Before and During the Nucleation Stage

YASUHIRO ARUGA and HIDENORI NAKO

The early precipitation of a Cu-Ni-P alloy during aging for 100 ks at 523 K and 623 K (250 °C and 350 °C) after solution treatment has been characterized using a three-dimensional atom probe (3DAP) and transmission electron microscopy (TEM). It is shown that the particles have a wide range of Ni/P ratios when they are relatively small, whereas larger ones exhibit a narrow distribution of the Ni/P ratio, approaching the ratio of approximately two. The threshold radii that show the steady Ni/P ratio are around 1.5 nm and 2.0 nm for the materials aged at 523 K and 623 K (250 °C and 350 °C), respectively. These values are in a reasonably good agreement with the critical nuclei radius estimated from classic nucleation theory. It is suggested that the particles with steady Ni/P ratios of approximately two are considered to be the equilibrium precipitates formed through nucleation, whereas the extremely fine particles with varying Ni/P ratios, detected by the 3DAP experiments, indicate subcritical clusters or embryos.

DOI: 10.1007/s11661-011-0950-2

© The Minerals, Metals & Materials Society and ASM International 2011

I. INTRODUCTION

COPPER alloy sheets are used widely for electrical terminals in automotive applications. The Cu-Ni-P alloy is one of the typical precipitation hardening type alloys, which are designed to exhibit both high strength and high electrical conductivity.^[1,2] Therefore, the characterization of strengthening phases is essential to understand these properties of the alloy. Some researchers have already confirmed the presence of equilibrium nickel phosphides, formed after aging at relatively high temperatures, using transmission electron microscopy (TEM) and selected area electron diffraction pattern analysis.^[1,3-5] Atom probe tomography (APT) is a powerful technique with sufficiently high spatial resolution in three dimensions to resolve the position and chemical identity of individual atoms.^[6,7] It has been applied successfully to study the earliest stages of decomposition in many alloy systems. Recently, Aruga *et al.*^[8-10] quantitatively characterized solute clustering during aging at 523 K (250 °C) in Cu-Ni-P alloys by means of three-dimensional atom probe (3DAP) and revealed that the clusters play a key role in the stress relaxation performance and age hardening behavior in Cu alloys.

However, our understanding of early-stage precipitation is limited, and there is a particular lack of quantitative information regarding the morphology, chemistry, and size-evolution of small, early stage precipitates. In this investigation, early precipitation of a Cu-Ni-P alloy during aging after solution treatment

has been explored. This research aims to characterize the early-stage precipitation in terms of size and chemical composition, and to suggest a link between the ratio of solute concentration in the features and the nucleation of precipitates.

II. EXPERIMENTAL PROCEDURE

An ingot of Cu-0.41Ni-0.11P (mass pct) alloy was manufactured using an air furnace, homogenized at 1223 K (950 °C) for 0.5 h, and hot rolled immediately down to 15 mm thickness, followed by cold rolling down to 0.80 mm thickness. The material was fully recrystallized and solution treated at 923 K (650 °C) for 20 seconds. The average grain size for the alloy was about 20 μm after water quenching. The alloy sheets were given an aging treatment for 100 ks at 523 K and 623 K (250 °C and 350 °C) in an air furnace. The alloys were aged in envelopes made of Cu foil filled with charcoal powder to prevent from oxidation.

TEM and an energy dispersive X-ray spectroscopy (EDS) were performed using a Hitachi HF-2200 (Hitachi, Ltd., Tokyo, Japan) at an operating voltage of 200 kV. The specimens for TEM were prepared by both thin foil and carbon extraction replica techniques. The foils were prepared using discs, 3 mm in diameter, which were mechanically ground to 0.12 mm thickness. The disks were then thinned electrolytically in a twin-jet polishing unit operating at 12 V using a Nimet solution (30 pct nitric acid and 70 pct methanol by volume) at 243 K (-30 °C). The replicas were prepared by etching in 1 pct ammonium acetate in methanol.

The specimens for 3DAP were cut from the sheets and electropolished using the standard two-stage method.^[7] The specimens were initially electropolished by a double layer technique with a solution of 10 vol pct orthophosphoric acid in water at 4 to 20 V AC at room

YASUHIRO ARUGA, Senior Researcher, and HIDENORI NAKO, Researcher, are with the Materials Research Laboratory, Kobe Steel, Ltd., 1-5-5 Takatsukadai, Nishi-ku, Kobe 651-2271, Japan. Contact e-mail: aruga.yasuhiro@kobelco.com

Manuscript submitted July 14, 2011.

Article published online October 19, 2011

temperature, and followed by electropolishing using a solution containing 10 g $\text{Na}_2\text{CrO}_4 \cdot 4\text{H}_2\text{O}$ in 100 mL acetic acid at 5V DC at room temperature.

3DAP analyses were carried out employing a LEAP 3000 HR instrument (CAMECA Instruments Inc., Madison, WI) at the University of Oxford. The analyses were practiced at a specimen temperature of 50 K (-223°C), a voltage pulse fraction (pulse voltage/steady-state voltage) of 20 pct, and a pressure in the specimen chamber below 10^{-8} Pa. Visualization and quantitative evaluation of the 3-D atom-by-atom data sets were performed with the IVAS software package (CAMECA Instruments Inc.). Three separate experimental runs were carried out for each heat treatment, and consistent results were obtained between runs.

III. RESULTS AND DISCUSSION

Figure 1(a) shows a TEM bright-field (BF) image of the material aged at 523 K (250°C) and a nanobeam electron diffraction pattern taken from the area of the BF image. The BF image shows a slight contrast arising from extremely fine particles. The diffraction pattern can be identified as an only Cu grain with a face-centered-cubic phase, but the diffraction pattern shows neither extra reflections nor diffuse scattering. Figure 1(b) shows a TEM BF image of the material aged at 623 K (350°C) and a nanobeam electron diffraction pattern taken from the area of the BF image. Spherical particles are observed in the BF image, but the diffraction pattern of the particle was not observed. The carbon replica extraction technique was used to extract the particles in the material aged at 623 K (350°C). The structure of the particles was analyzed from the diffraction patterns of individual particles, without the effect of matrix on the electron diffraction. Figure 1(c) shows a typical nanobeam electron diffraction pattern of extracted particle. From the analysis of the diffraction pattern and the corresponding EDS analysis, the particles could be identified as tetragonal Ni_{12}P_5 .^[11]

APT relies on the combination of field evaporation, time-of-flight spectroscopy, and position sensitive detection. Specimens in the shape of sharp needles are subjected to electric fields sufficient to promote ionization of surface atoms.^[12] As the specimen is field evaporated, its radius r_t normally increases, and hence, the magnification decreases. Because it is impractical to measure the radius of the specimen after each ion is field evaporated, it is estimated from the evaporation voltage V applied to the specimen with the following relationship.

$$r_t = \frac{V}{kF} \quad [1]$$

where F is the evaporation field at the apex of the specimen and k is the geometrical field factor. The detector position can be related to the initial position of the atom on the needle apex assuming a simple projection law. The sequence of evaporation is used to provide depth information, and the overall evaporated

material can therefore be reconstruction in three dimensions. Time-of-flight measurements provide a value for the mass/charge ratio of each evaporated ion and therefore their identity.^[13] To reconstruct the volume accurately, the initial specimen radius of curvature was adjusted based on the observation of identified planes in the reconstruction in this work. Reconstructed 3DAP maps are shown in Figure 2. The Ni and P atoms are depicted by points, whereas no Cu atoms are shown, to illustrate the distribution of Ni and P atoms more clearly. Some indications of phase separation are observed in the material aged at 523 K (250°C) (Figure 2(a)). It is observed that the material aged at 623 K (350°C) (Figure 2(b)) exhibits distinct evidence of Ni-P clustered features.

To make reasonably accurate measurements and allow quantification of the atomic scale microstructural changes, the maximum separation method^[14,15] was used to select discrete regions enriched in solute. This was carried out by grouping together solute Ni and P atoms within a given distance d_{max} of one another ($d_{\text{max}} = 0.6$ nm in the current study). Then, by removing all the groups that contained less than $N_{\text{min}} = 5$ solute atoms, the map of solute-rich regions was obtained. N_{min} and d_{max} values were chosen so that no particles were observed in a random solid solution of the same composition. This was tested by assigning the atom identities randomly to the positions in the data and testing different N_{min} and d_{max} values on this randomized data. Using these values, the size distribution and chemistry of the particles were evaluated.

The spatial distributions of the particles that are easily observed by applying the maximum separation method using $N_{\text{min}} = 5$ are given in Figures 2(c) and (d). The radius of gyration and the associated Guinier radius are parameters commonly used in the literature to define the sizes of particles.^[7] A standard measure of the size of a feature is the radius of gyration

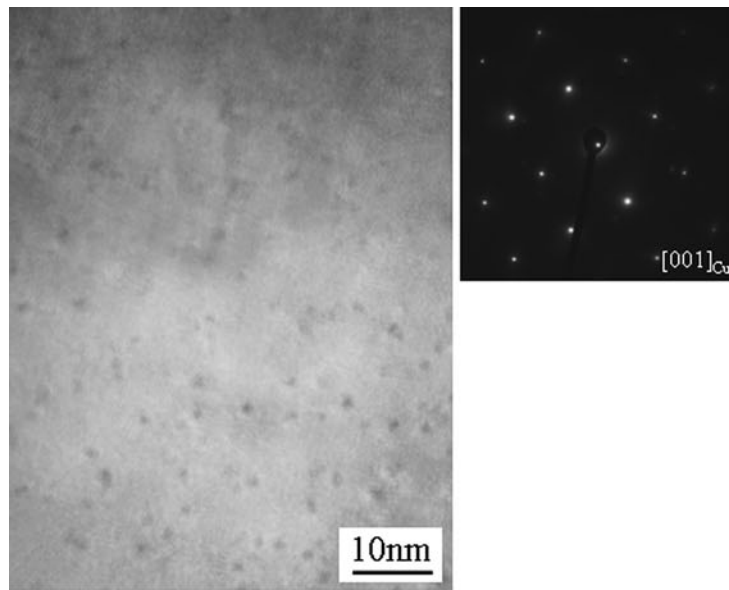
$$l_g = \sqrt{\frac{\sum_{i=1}^n (x_i - \bar{x})^2 + (y_i - \bar{y})^2 + (z_i - \bar{z})^2}{n}} \quad [2]$$

where x_i , y_i , and z_i are the spatial coordinates of each atom; n is the number of atoms in the feature; and \bar{x} , \bar{y} , and \bar{z} are the coordinates of the center of mass of the feature. The radius of gyration l_g is always smaller than the actual size of the feature. Hence, the Guinier radius r_G is often the reported value, where the two are related in the following way:

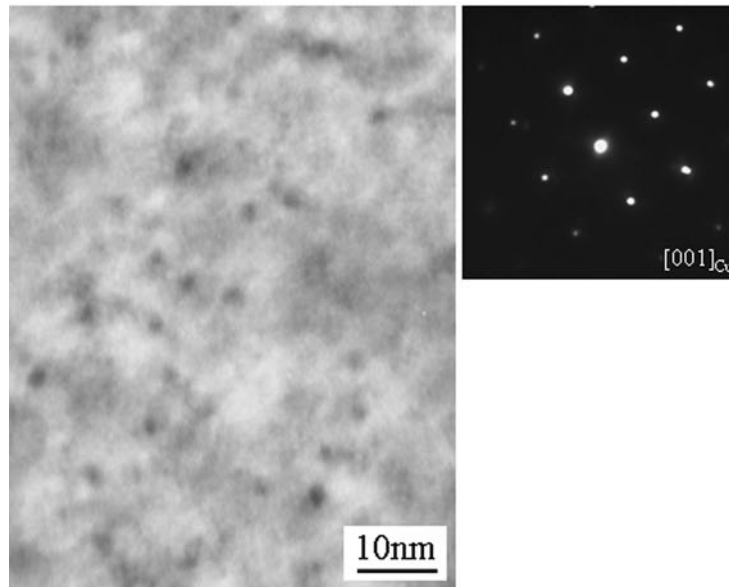
$$r_G = \sqrt{\frac{5}{3}} \cdot l_g \quad [3]$$

The size distributions of the particles are shown in Figure 3. A clear peak in the number fraction can be observed at approximately 0.7 nm in the Guinier radius for the material aged at 523 K (250°C), whereas the material aged at 623 K (350°C) has a relatively broad distribution.

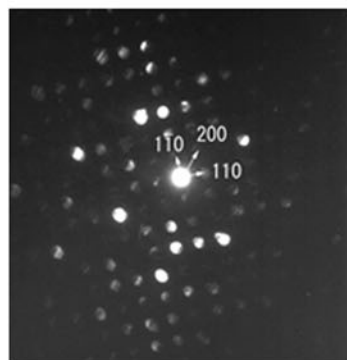
The Ni/P ratios of the particles have been evaluated by taking the Ni and P atoms involved in particles



(a)



(b)



(c)

Fig. 1—(a) TEM BF image and nanobeam electron diffraction pattern in the Cu-Ni-P alloy aged at 523 K (250 °C) for 100 ks. (b) TEM BF image and nanobeam electron diffraction pattern in the Cu-Ni-P alloy aged at 623 K (350 °C) for 100 ks. (c) Nanobeam electron diffraction pattern of a particle in a carbon replica of the material aged at 623 K (350 °C).

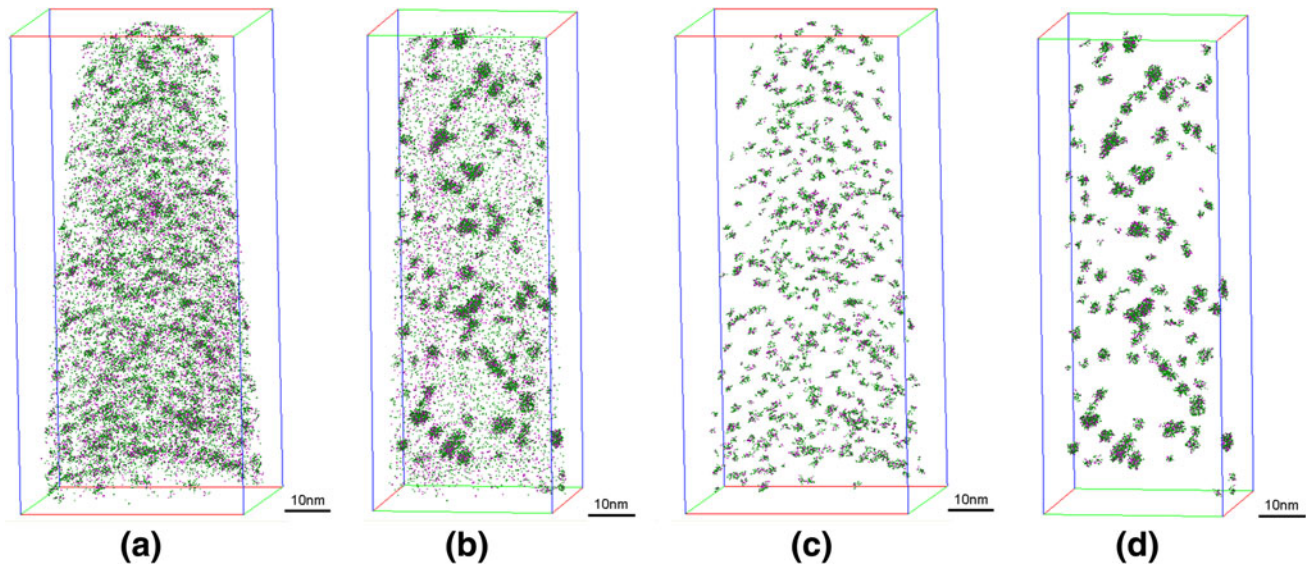


Fig. 2—(a) 3-D APT map (green = Ni atoms and pink = P atoms) of the Cu-Ni-P alloy aged at 523 K (250 °C) for 100 ks. (b) 3-D APT map (green = Ni atoms and pink = P atoms) of the Cu-Ni-P alloy aged at 623 K (350 °C) for 100 ks. (c) 3-D APT map (green = Ni atoms and pink = P atoms) of clustered data from (a). (d) 3-D APT map (green = Ni atoms and pink = P atoms) of clustered data from (b).

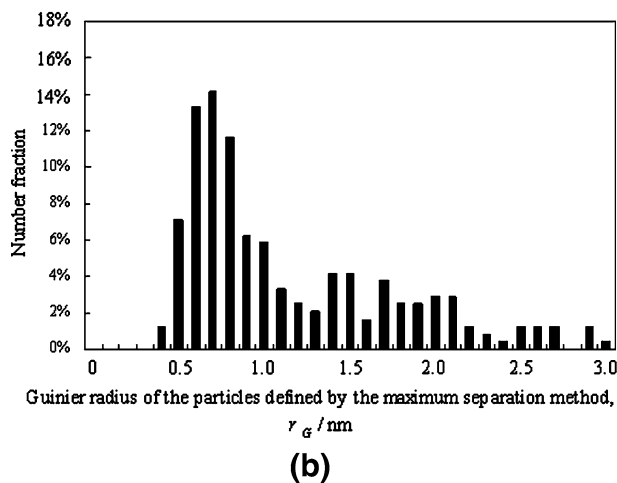
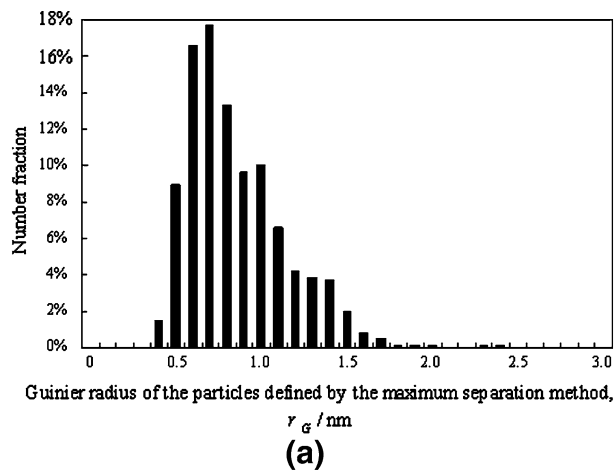


Fig. 3—Size distribution of the particles in the Cu-Ni-P alloy aged at (a) 523 K (250 °C) for 100 ks and (b) 623 K (350 °C) for 100 ks.

defined by the maximum separation method. Figure 4 shows the relationship between the size and Ni/P ratio of the particles for the material aged at 523 K (250 °C) (Figure 4(a)) and 623 K (350 °C) (Figure 4(b)). It is shown that the particles have a range of Ni/P ratios, especially when they are relatively small. In contrast, larger ones exhibit a narrow distribution of Ni/P ratios, approaching the ratio of approximately two.

The particles observed in the material aged at 623 K (350 °C) have been identified as a Ni_{12}P_5 phase from the analysis of the diffraction patterns as indicated previously. According to the copper-rich corner of the Cu-Ni-P equilibrium diagrams recently reported by Hino *et al.*,^[16] it is expected that the most probable dominant phase for the composition of the current work at 523 K and 623 K (250 °C and 350 °C) is Ni_{12}P_5 , and a second possible phase is Ni_2P . It is believed that the ratio approaches a value identical to that of the equilibrium phase as the particles enlarge during aging. The threshold radii, beyond which a steady Ni/P ratio (range, between 1.5 to 2.9) is observed, are approximately 1.5 nm and 2.0 nm for the materials aged at 523 K and 623 K (250 °C and 350 °C), respectively.

Classic nucleation theory^[17,18] determines the minimum stable size of the nuclei, which are called critical nuclei. The theory supposes a uniform solute distribution throughout the matrix and nuclei. The size of the critical nuclei varies with temperature. As the temperature is decreased, the critical radius for nucleation rapidly decreases in size, as does the energy necessary to form the critical embryo. The critical nuclei radius r^* can be expressed by the following equation^[17]:

$$r^* = -\frac{2\sigma}{(\Delta G_v - \Delta G_s)} \quad [4]$$

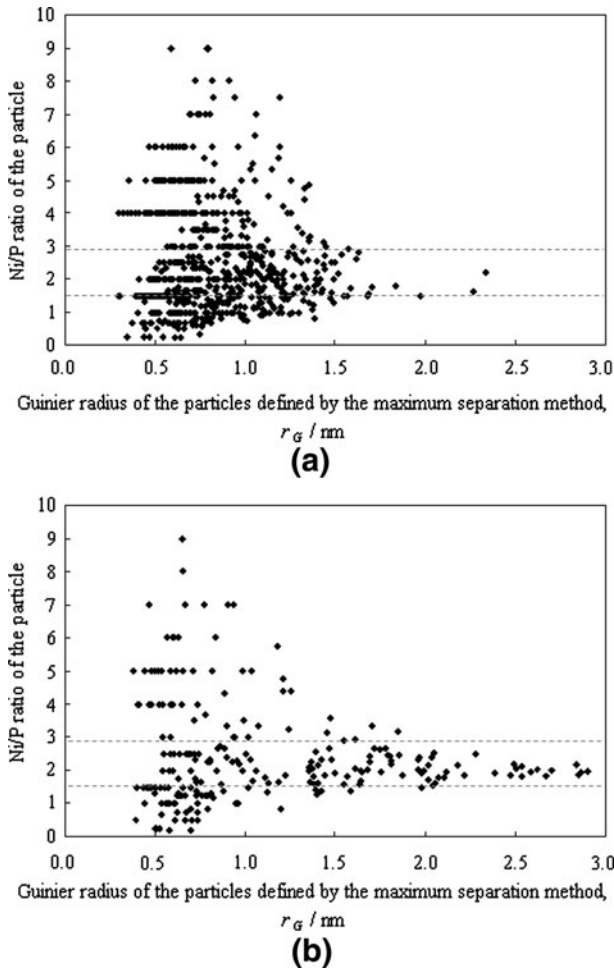


Fig. 4—Size dependence of Ni/P ratio of particles in the Cu-Ni-P alloy aged at (a) 523 K (250 °C) for 100 ks and (b) 623 K (350 °C) for 100 ks.

where σ is the interfacial energy of the precipitate, ΔG_v is driving force^[19] for nucleation and ΔG_S is elastic strain energy. It must be noted that this theory assumes isotropic interfacial and elastic strain energy. It cannot be applied if both or either energy has anisotropy. It is reported that the coherency interfacial energy is between 0.05 and 0.2 J/m².^[20] The value of σ is taken as 0.14 J/m² in the current work. Fujiwara^[21] showed that the simulated value is in good agreement with experimental results in the case of coherent precipitates in Cu alloys. The driving forces for nucleation at 523 K and 623 K (250 °C and 350 °C), calculated using Thermo-Calc software (Thermo-Calc Software, Inc., McMurray, PA)^[22] with the thermodynamic database of the Cu-Ni-P system,^[16] are 33 and 26 kJ/mol (kJ per mol of total atoms), respectively. The elastic strain energy ΔG_S is estimated as follows.

First, a spherical volume (radius = R_M) of matrix is virtually extracted and transformed into a spherical volume of Ni₁₂P₅ (radius = R_P), and the spherical Ni₁₂P₅ is virtually pushed into the original spherical volume of matrix. Then, ΔG_S is obtained as strain

energy associated with the push-in. The strain energies of the matrix and precipitate (Ni₁₂P₅) were calculated as below.

The radius of Ni₁₂P₅ after push-in, R^* and the elastic strain energy of the matrix per unit volume E_M are described as

$$R^* = \frac{2Y_M(1-2\nu_P)R_M + Y_P(1+\nu_M)R_P}{2Y_M(1-2\nu_P) + Y_P(1+\nu_M)} \quad [5]$$

$$E_M = \frac{3}{4} \frac{1+\nu_M}{Y_M} \left(\frac{R^*}{r} \right)^6 P_*^2 \quad [6]$$

where Y is the Young's modulus and ν is the Poisson's ratio. The suffixes "M" and "P" refer to the matrix and the precipitate (Ni₁₂P₅), respectively. r is the distance from the center of the spherical Ni₁₂P₅. P_* is the interacting stress and is expressed by Eq. [7]^[23]

$$P_* = \frac{2Y_M}{1+\nu_M} \frac{R_M - R^*}{R^*} \quad [7]$$

From Eqs. [6] and [7], the elastic strain energy of the matrix ΔG_M can be written as

$$\begin{aligned} \Delta G_M &= \int_{R^*}^{\infty} E_M 4\pi r^2 dr \\ &= 4\pi \frac{Y_M}{1+\nu_M} (R_M - R^*)^2 R^* \end{aligned} \quad [8]$$

Considering Ni₁₂P₅, the applied stress (σ_r , σ_θ , and σ_ϕ) and the strain (ε_r , ε_θ , and ε_ϕ) are given by

$$\sigma_r = \sigma_\theta = \sigma_\phi = P_* \quad [9]$$

$$\varepsilon_r = \varepsilon_\theta = \varepsilon_\phi = \frac{1-2\nu_P}{Y_P} P_* \quad [10]$$

in spherical coordinates. The elastic strain energy of the Ni₁₂P₅ per unit volume ΔG_{PV} is obtained as

$$\begin{aligned} \Delta G_{PV} &= \frac{1}{2} (\sigma_r \varepsilon_r + \sigma_\theta \varepsilon_\theta + \sigma_\phi \varepsilon_\phi) \\ &= \frac{3}{2} \frac{1-2\nu_P}{Y_P} P_*^2 \end{aligned} \quad [11]$$

Then, the precipitation strain energy per unit volume ΔG_{SV} is given

$$\Delta G_{SV} = \frac{\Delta G_M}{4\pi R_*^3 / 3} + \Delta G_{PV} \quad [12]$$

Assuming that Ni in a Cu matrix is a substitutional element and P is interstitial, R_M and R_P satisfy the following equation:

$$\frac{4\pi R_M^3 / 3}{V_M} \times \frac{12+5}{12} = \frac{4\pi R_P^3 / 3}{V_P} \quad [13]$$

where V_M and V_P are the molar volumes of Cu matrix and $Ni_{12}P_5$, respectively. Equation [12] becomes

$$\Delta G_{SV} = 3Y_M Y_P \{2Y_M(1 - 2v_P) + Y_P(1 + v_M)\} \left\{ \frac{\sqrt[3]{12V_M} - \sqrt[3]{17V_P}}{2Y_M(1 - 2v_P)\sqrt[3]{12V_M} + Y_P(1 + v_M)\sqrt[3]{17V_P}} \right\}^2 \quad [14]$$

by using Eqs. [5] through [8], [11], and [12]. Thus, we obtain ΔG_S by multiplying ΔG_{SV} by V_P .

We used $v_M = 0.34$,^[24] $Y_P = 192.8$ GPa,^[25] and $V_P = 1.14 \times 10^{-4}$ m³/mol.^[26] Y_M was calculated from the rigidity modulus of Cu, $G_M = 44.8$ GPa,^[24] and following the equation

$$Y_M = 2G_M(1 + v_M) \quad [15]$$

V_M was led to be 7.11×10^{-6} m³/mol from the lattice parameter of Cu, 0.36 nm. v_P was assumed to be 0.3.

The value of the elastic strain energy ΔG_S calculated is 12 kJ/mol. When this value is substituted into Eq. [4], the critical nuclei radii r^* at 523 K and 623 K (250 °C and 350 °C) are 1.5 and 2.2 nm, respectively. These are in a reasonably good agreement with the threshold Guinier radii, which correspond to steady Ni/P ratios in the 3DAP analysis.

When it is assumed that both Ni and P are substitutional elements, Eq. [13] should be written as in Eq. [16]

$$\frac{4\pi R_M^3/3}{V_M} = \frac{4\pi R_P^3/3}{V_P} \quad [16]$$

and ΔG_S is estimated to be 0.5 kJ/mol. Based on this result, the r^* s at 523 K and 623 K (250 °C and 350 °C) are found to be 1.0 and 1.3 nm, respectively. However, it is obvious that the Ni/P ratios of particles at these radii in the 3DAP analysis are wildly different. This may imply that the assumption that Ni and P are substitutional is inadequate.

Thus, it is speculated that the particles which have steady Ni/P ratios around two are the equilibrium precipitates formed through nucleation. In contrast, we believe that the extremely fine particles with varying Ni/P ratios, detected by the 3DAP experiments, indicate subcritical clusters or embryos. The accurate comparison of the crystal structure of these small particles is difficult because of an intrinsic limitation of detection efficiency in the APT and the insufficient resolution of TEM, but future studies are needed.

IV. CONCLUSIONS

Early precipitation of a Cu-0.41Ni-0.11P (mass pct) alloy during aging for 100 ks at 523 K and 623 K (250 °C and 350 °C) after solution treatment has been characterized in terms of the size and chemical composition of the particles. A 3DAP analysis showed that the particles defined by the maximum separation method have a wide range of Ni/P ratios when they are relatively small, whereas larger ones exhibit a narrow distribution of the Ni/P ratio, approaching the

ratio of approximately two. The threshold radii that show the steady Ni/P ratio are approximately 1.5 nm and 2.0 nm for the materials aged at 523 K and 623 K (250 °C and 350 °C), respectively. These values are in a reasonably good agreement with the critical nuclei radius estimated from classic nucleation theory. Therefore, it is suggested that the particles with steady Ni/P ratios at approximately two are considered to be the equilibrium precipitates formed through nucleation, whereas the extremely fine particles with varying Ni/P ratios, detected by the 3DAP experiments, indicate subcritical clusters or embryos.

ACKNOWLEDGMENTS

The authors thank Drs. D.W. Saxey and E.A. Marquis for their assistance in performing the 3DAP experiments. Mr. S. Namba and Dr. T. Murakami are warmly thanked for fruitful discussions.

REFERENCES

1. J. Miyake and M.E. Fine: *Acta Metall. Mater.*, 1992, vol. 40, pp. 733–41.
2. J. Miyake, G. Ghosh, and M.E. Fine: *MRS Bull.*, 1996, vol. 21, pp. 13–18.
3. W.H. Tian, C.K. Yan, and M. Nemoto: *Acta Metall. Sinica*, 2003, vol. 16, pp. 155–60.
4. M. Murayama, A. Belyakov, T. Hara, Y. Sasaki, K. Tsuzaki, M. Okubo, M. Eto, and T. Kimura: *J. Electron. Mater.*, 2006, vol. 35, pp. 1787–92.
5. J.-S. Byun, J.H. Choi, and D.N. Lee: *Scripta Mater.*, 2000, vol. 42, pp. 637–43.
6. M.K. Miller, A. Cerezo, M.G. Hetherington, and G.D.W. Smith: *Atom Probe Field Ion Microscopy*, Oxford University Press, Oxford, UK, 1996.
7. M.K. Miller: *Atom Probe Tomography*, Kluwer Academic/Plenum Publishers, New York, NY, 2000.
8. Y. Aruga, D.W. Saxey, E.A. Marquis, H. Shishido, Y. Sumino, A. Cerezo, and G. D.W. Smith: *Metall. Mater. Trans. A*, 2009, vol. 40A, pp. 2888–2900.
9. Y. Aruga, D.W. Saxey, E.A. Marquis, H. Shishido, Y. Sumino, A. Cerezo, and G.D.W. Smith: *Mater. Trans.*, 2010, vol. 51, pp. 1802–08.
10. Y. Aruga, D.W. Saxey, E.A. Marquis, A. Cerezo, and G.D.W. Smith: *Ultramicroscopy*, 2011, vol. 111, pp. 725–29.
11. S. Rundqvist and E. Larsson: *Acta Chem. Scand.*, 1959, vol. 13, pp. 551–60.
12. D.G. Brandon: *Phil. Mag.*, 1966, vol. 14, pp. 803–20.
13. J.A. Panitz, S.B. McLane, and E.W. Muller: *Rev. Sci. Instrum.*, 1969, vol. 40, pp. 1321–24.
14. J.M. Hyde: Ph.D. Dissertation, Oxford University, Oxford, UK, 1993.
15. J.M. Hyde and C.A. English: *Materials Research Symposia*, G.E. Lucas, L. Snead, M.A. Kirk, and R.G. Elliman, eds., Materials Research Society, Pittsburgh, PA, 2001, vol. 650, p. R6.6.
16. M. Hino, H. Shishido, Y. Aruga, S. Namba, S. Iikubo, and H. Ohtani: *Collected Abstracts of the 2010 Autumn Meeting of Japan Inst. Metals*, Japan Inst. Metals, Sendai, Japan, 2010, p. 444.
17. D.A. Porter and K.E. Easterling: *Phase Transformations in Metals and Alloys*, Van Nostrand Reinhold Co. Ltd, UK, 1981, p. 266.
18. R. Becker and W. Döring: *Ann. Phys.*, 1935, vol. 24, p. 719.
19. H.I. Aaronson: *Lectures on the Theory of Phase Transformations*, AIME, New York, NY, 1975, p. 24.
20. J.M. Howe: *Interfaces in Materials*, Wiley, New York, NY, 1997, p. 378.
21. H. Fujiwara: *Furukawa Review*, 2001, vol. 108, pp. 47–54.

22. B. Sundman, B. Jansson, and J.-O. Andersson: *CALPHAD*, 1985, vol. 9, pp. 153–90.
23. T. Minote and S. Torizuka: *Use of Fine Inclusions in Microstructure Control of Steels—Literature Survey and Preliminary Study of Controlling Mechanism by Computer Model*, The Iron and Steel Institute of Japan, Tokyo, Japan, 1995, pp. 65–74.
24. A. Kelly and G.W. Groves: *Crystallography and Crystal Defects*, Addison-Wesley, Reading, MA, 1970, p. 163.
25. D. Zhao, L. Zhou, Y. Du, A. Wang, Y. Peng, Y. Kong, C.-S. Sha, Y. Ouyang, and W. Zhang: *CALPHAD*, 2011, vol. 35, pp. 284–91.
26. W. Liu, X. Sun, L.R. Pederson, O.A. Marina, and M.A. Khaleel: *J. Power Sources*, 2010, vol. 1950, pp. 7140–45.